PERGAMON

Engineering Fracture Mechanics 65 (2000) 1–14

Engineering Fracture Mechanics

www.elsevier.com/locate/engfracmech

Surface crack subject to mixed mode loading

M.Y. He[a], J.W. Hutchinson[b,*]

[a]*Materials Engineering Department, University of California, Santa Barbara, CA 93106, USA*
[b]*Division of Engineering and Applied Sciences, Applied Sciences, 315 Pierce Hall, 29 Oxford Street, Harvard University, Cambridge, MA 02138, USA*

Received 19 April 1999; received in revised form 2 November 1999; accepted 10 November 1999

Abstract

Stress intensity factor distributions at the edge of semi-circular and semi-elliptical surface cracks are obtained for cracks aligned perpendicular to the surface of a semi-infinite solid subject to remote shear parallel to the plane of the crack. Mixed mode conditions along the crack edge are characterized. Application to fatigue crack thresholds in mixed mode is discussed.

Keywords: Surface crack; Modes II and III; Fatigue crack growth; Fatigue threshold

1. Introduction

Surface crack solutions are widely used in applications of fracture mechanics to fatigue and monotonic loadings. A semi-elliptical surface crack lying perpendicular to the surface and subject to applied stresses with no shear component parallel to the crack experiences mode I conditions around its edge. It is usually tacitly assumed that this orientation is the critical one. Whether this orientation is critical for designs based on fatigue crack thresholds has been called into question by some recent experimental data [1–3] which indicate that long crack threshold conditions may be lower under mixed mode than under mode I. It is this observation which motivates the present study of the mixed mode stress intensity factors for cracks at surfaces under general remote uniform stressing. Attention is directed to cracks which are perpendicular to the surface. The results presented below supplement the mode I stress intensity factors of Raju and Newman [4,5] for cracks perpendicular to the surface and by Noda and Miyoshi [6] and Noda et al. [7] for cracks inclined to the surface. The only other results in

* Corresponding author. Tel.: +1-617-495-2848; fax: +1-617-495-9837.
E-mail address: hutchinson@husm.harvard.edu (J.W. Hutchinson).

0013-7944/00/$ - see front matter
PII: S0013-7944(99)00129-0

the literature on the mixed mode crack problem analysed in this paper appears to be prelimary results in a paper by Murikami [8] which will be discussed later.

The problem addressed here is depicted in Fig. 1(a). An isotropic elastic half-space with a semi-circular or semi-elliptical crack in the (x_1, x_3) plane is subject to a remote uniform stress specified by the components $(\sigma^0_{11}, \sigma^0_{22}, \sigma^0_{12})$. The crack is not influenced by the component σ^0_{11} since this component produces no traction on the crack plane. The component σ^0_{22} induces a mode I stress intensity factor distribution along the crack edge which is available in Ref. [5]. The component σ^0_{12} induces both mode II and mode III intensity factor distributions. It is these distributions which will be computed and characterized in this paper. The solution for arbitrary uniform remote stressing is obtained by superposition of the distributions due to σ^0_{22} and σ^0_{12}. A crack inclined to a remote tensile field, as shown in Fig. 1(b), is a special case of this solution. This case will be used to illustrate potential mixed mode effects later in the paper.

2. Solution for shear stress applied parallel to the crack

Consider semi-elliptical cracks in the (x_1, x_3) plane with depth a and half-length c at the surface(Fig. 1(a)). The only nonzero remote stress component is σ^0_{12}. The Young's modulus of the elastic material is E and the Poisson's ratio is ν. The symmetry of the geometry and anti-symmetry of the loading dictates that the mode I stress intensity factor, K_{I}, vanishes along the crack edge. The mode II and mode III intensity factors, K_{II} and K_{III}, vary along the crack edge and will be regarded as functions of the angle φ defined in Fig. 1(a). These factors are odd and even functions, respectively, with respect to the deepest point of the crack, $\varphi = \pi/2$. It will be seen that K_{II} is largest in magnitude near the surface, while K_{III} is largest where the crack penetrates most deeply into the body.

2.1. A reference solution

A useful reference solution is that for the similarly aligned and loaded elliptical crack in an infinite

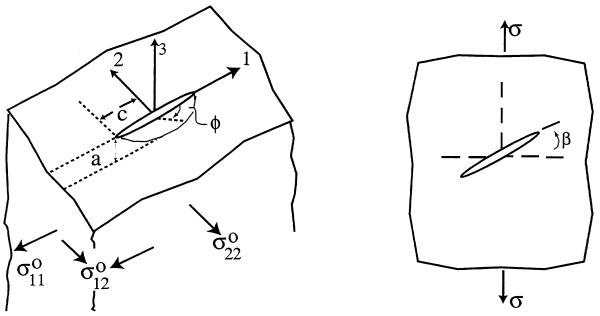

Fig. 1. (a) Semi-elliptical surface crack in a semi-infinite isotropic elastic solid subject to uniform remote stresses $(\sigma^0_{11}, \sigma^0_{22}, \sigma^0_{12})$. The present paper considers the shear loading σ^0_{12} which induces mode II and III stress intensities along the crack front. Solutions for the mode I problem due to σ^0_{22} exist in the literature. The stress component σ^0_{11} has no influence on the stress intensity factors. (b) Surface crack aligned obtusely to the remote tensile field.

solid [9–11]. This is an exact solution given by

$$K_{\mathrm{II}}^{0} = \frac{\sigma_{12}^{0}\sqrt{\pi a}k^{2}(a/c)\cos\varphi}{B\left[\sin^{2}\varphi + (a/c)^{2}\cos^{2}\varphi\right]^{1/4}}$$

$$K_{\mathrm{III}}^{0} = \frac{\sigma_{12}^{0}\sqrt{\pi a}k^{2}(1-\nu)\sin\varphi}{B\left[\sin^{2}\varphi + (a/c)^{2}\cos^{2}\varphi\right]^{1/4}} \tag{1}$$

where

$$k^{2} = 1-(a/c)^{2}, \qquad B = (k^{2}-\nu)E(k) + \nu(a/c)^{2}K(k)$$

with elliptic integrals defined by

$$E(k) = \int_{0}^{\pi/2}\sqrt{1-k^{2}\sin^{2}\varphi}\,\mathrm{d}\varphi, \qquad K(k) = \int_{0}^{\pi/2}\frac{\mathrm{d}\varphi}{\sqrt{1-k^{2}\sin^{2}\varphi}}$$

The maximum values of the reference intensity factors will be used for scaling the surface crack solutions:

$$\left(K_{\mathrm{II}}^{0}\right)_{\varphi=0} = \sigma_{12}^{0}\sqrt{\pi a}k^{2}(a/c)^{1/2}/B$$

$$\left(K_{\mathrm{III}}^{0}\right)_{\varphi=\pi/2} = \sigma_{12}^{0}\sqrt{\pi a}k^{2}(1-\nu)/B \tag{2}$$

Numerical values for these factors are given in Table 1 for a range of c/a and ν.

Table 1
Maximum values of the reference intensity factors from Eq. (2)

ν	c/a	$(K_{\mathrm{II}}^{0})_{\varphi=0}/\sigma_{12}^{0}\sqrt{\pi a}$	$(K_{\mathrm{III}}^{0})_{\varphi=\pi/2}/\sigma_{12}^{0}\sqrt{\pi a}$
0	1	0.637	0.637
0	1.5	0.618	0.756
0	2	0.584	0.826
0	3	0.518	0.898
0.2	1	0.707	0.566
0.2	1.5	0.710	0.695
0.2	2	0.685	0.775
0.2	3	0.623	0.863
0.3	1	0.749	0.525
0.3	1.5	0.767	0.657
0.3	2	0.750	0.743
0.3	3	0.693	0.841
0.5	1	0.849	0.425
0.5	1.5	0.913	0.559
0.5	2	0.927	0.655
0.5	3	0.895	0.775

2.2. Behavior at the corner of the crack at the free surface ($\varphi = 0$)

Under general stressing, the stress field along interior points of the crack edge is the superposition of the conventional mode I, II and III fields, which are characterized by an inverse square root dependence on the distance from the tip. At the point where the crack edge intersects the free surface, a three-dimensional corner singularity exists [12–14]. With R as the distance from the corner point, the singular stresses associated with the symmetric field (mode I) become unbounded as R diminishes according to

$$\sigma \propto R^{-S_s} \tag{3a}$$

while the stresses in the anti-symmetric fields (modes II and III) satisfy

$$\sigma \propto R^{-S_a} \tag{3b}$$

Plots of S_s and S_a as a function of ν are given in Fig. 2. Except for $\nu = 0$, the corner singularity of the mode I field is weaker, and that of the anti-symmetric modes is stronger, than inverse square root behavior. The relationship between the corner and interior singularity strengths and the character of the full solution has been examined for a specific three-dimensional, mode I problem [15] (e.g. the through-crack in a finite thickness plate). The effective zone of dominance of the corner singularity comprises a very small fraction of the crack edge. Over most of the crack edge, the stress intensity factor associated with the inverse square root behavior governs the stresses and strains, although the distance from the crack tip for which local plane strain conditions are achieved is a small fraction of the plate thickness.

The effect of the strong corner singularity (3b) on the mode II and III stress intensity factor distributions for the problem considered here will be apparent. However, no attempt has been made to incorporate the corner singularity (3b) in the representation of the numerical results for the distributions. High resolution accuracy at the corner may not be worth pursuing, in any case, because the geometry where the crack intersects the surface is expected to adjust under loading so as to ameliorate the stronger singularity.

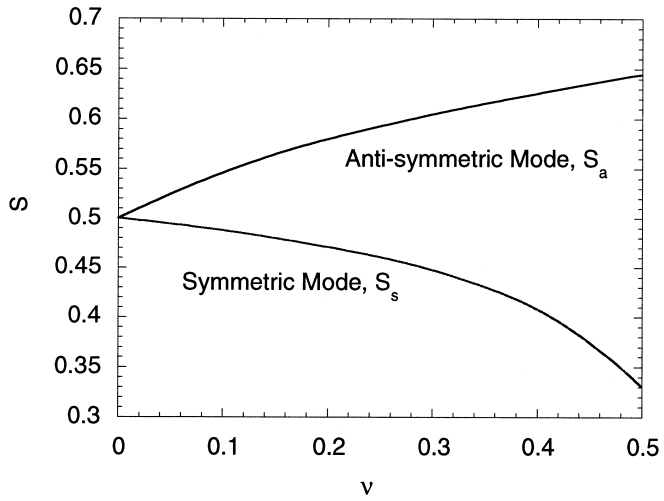

Fig. 2. Dependence of the singularity exponents (3) for stress fields at the corner where the crack intersects the surface of the half space, S_s for the mode I and S_a, for mode II and III, respectively [14].

2.3. Finite element meshes

A three-dimensional finite-element analysis has been used to calculate the strain energy release rate and the mode II and III stress-intensity factor distributions along the surface crack front. The finite-element mesh for a semi-elliptical crack can be obtained from that for a semi-circular crack by an elliptical transformation. This transformation is convenient for generating the mesh, and it has advantages for the evaluation of the energy release rate because of its orthogonal nature. The element sides along the crack front are perpendicular to the front. This increases the accuracy of strain energy release rate (for crack advance in the plane of the crack) when it is evaluated numerically using the J-integral with the domain integral method [16]. Specifically, the (x, y, z) Cartesian coordinates of a node in the semi-circular case become the (x', y', z') coordinates of the same node in the semi-elliptical case when

$$x = a\eta\cos\varphi \tag{4a}$$

$$y = a\eta\sin\varphi \tag{4b}$$

such that

$$x' = \cos\varphi\left(c^2 + \left(\eta^2 - 1\right)a^2\right)^{1/2}$$

$$y' = y$$

$$z' = z \tag{5}$$

for $c/a > 1$. The relation between circular arcs and radial lines in the (x, y) plane of the semi-circular crack and ellipses and hyperbolas, respectively, in the (x', y') plane of the semi-elliptical crack is illustrated in Fig. 3(a). While the total energy release rate, G, was evaluated using J-integral method, the individual stress intensity factors were determined by fitting the near-tip displacement fields for mode II and III to the crack face displacement components from the numerical solution.

A general purpose finite element code, ABAQUS was used for the analysis. Twenty-node quadratic isoparametric brick elements were employed to model the problem. Symmetry and anti-symmetry conditions were exploited such that only one quarter of the half space was meshed. Several meshes were used to gauge accuracy (see Fig. 3(b) for a representative mesh). The coarse mesh used in the convergence study had 864 element and 4698 nodes. A finer mesh, which had 1728 elements and 9002 nodes, was used to generate the main results in the paper.

To evaluate the quality of the mesh, the energy release rate was calculated for an embedded elliptical crack in the full space under uniform remote shear stress using the same mesh employed to produce solutions for the surface crack problems. The results were within 0.5% of the exact solution from Eq. (1).

Examples of the numerical solution for the stress intensity distributions are presented in Fig. 4 for the semi-circular crack ($c/a = 1$). Complications at the corner at $\varphi = 0$ do not appear in Fig. 4(a) when Poisson's ratio vanishes. A fine mesh has been employed in the vicinity of the corner, as revealed by the points in the figure where the stress intensity factors have been evaluated. The solution to the semi-circular surface crack is very close to that for the penny-shaped crack in the infinite body (1) when $\nu = 0$. The effect of the corner singularity is evident in Fig. 4(b) for $\nu = 0.3$. In the vicinity of the corner, K_{III} does not go smoothly to zero, and K_{II} displays distinctly non-uniform behavior for $\varphi < 0.1(\cong 5^\circ)$,

consistent with the existence of a corner singularity Eq. (3) stronger than the square root dependence in the interior. The effect of the finite element mesh is also evident in Fig. 4(b). The coarse mesh provides accuracy almost equal to that of the moderately fine mesh for $\varphi > 0.35(\cong 20^\circ)$, but provides inadequate resolution nearer to the corner.

Another exploration of meshing is presented in Fig. 5, which shows the energy release rate along the front of a semi-circular surface crack normalized by the corresponding distribution, $G_0(\varphi)$, from Eq. (1) for the penny-shaped crack in the infinite body. The rates are for crack advance in the plane of the crack. The two meshes used have the same number of elements. One is the fine mesh described above, and the other employs smaller elements near the free surface and larger elements along the edge in the interior. The J-integral has been used to compute the energy release rate at points along the front. For $\nu = 0.3$, the evaluation points for the mesh with the finest resolution at the corner are indicated by solid diamonds in Fig. 5, while a curve has been drawn for the results from the other mesh. The role of the strong corner singularity for $\varphi < 0.1(\cong 5^\circ)$ is brought out clearly by the trend near the corner. (The results for $\nu = 0$, which have not been plotted, are virtually identical to those for the penny-shaped crack in the infinite solid with G going smoothly to the limit at the corner.) For $\nu = 0.3$, both meshes capture the upturn in the energy release at the corner for $\varphi < 0.1(\cong 5^\circ)$. Apart from the behavior very near the corner, the distribution for the penny-shaped crack is within 5% of that of the surface crack. Whether the highly localized behavior at the corner has important physical implications will have to await comparison with observations. In this paper, no attempt has been made to provide accurate

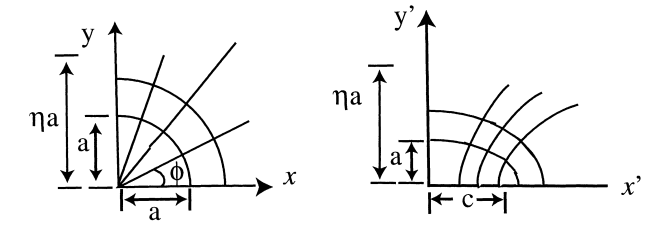

a) Semi-circular Semi-elliptical

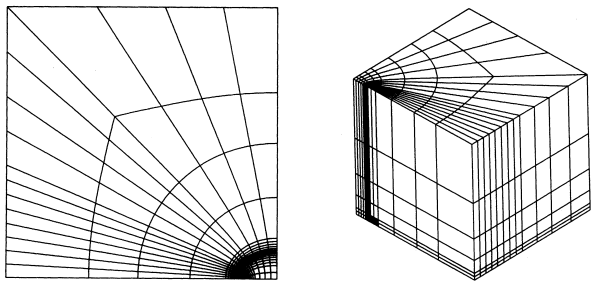

b)

Fig. 3. (a) Coordinates used to generate the mesh. (b) Representative finite element mesh for $c/a = 1.5$.

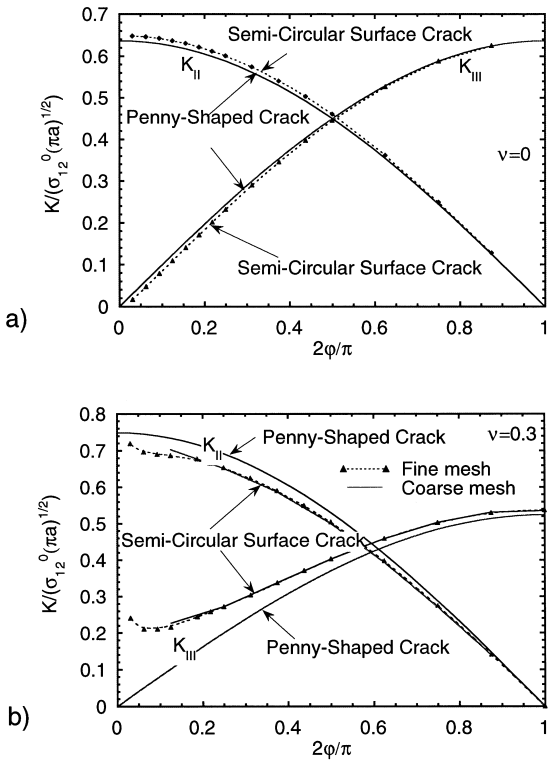

Fig. 4. Distributions of the stress intensity factors for (a) $\nu = 0$ and (b) $\nu = 0.3$ for the semi-circular surface crack and the penny-shaped crack in the infinite solid, both subject to nonzero σ_{12}^0. Comparison between predictions of coarse and fine meshes are shown in (b).

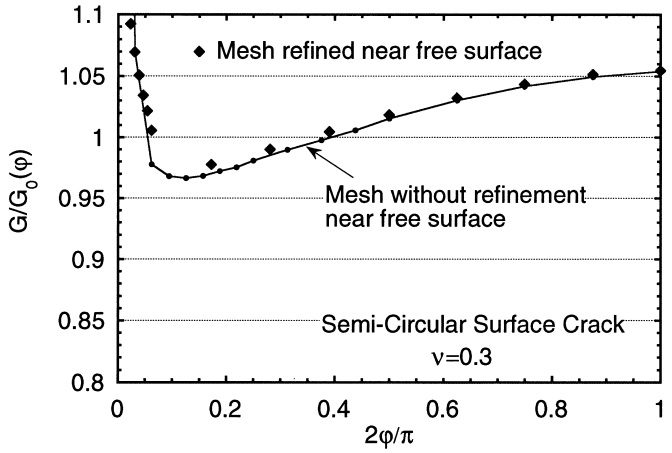

Fig. 5. Energy release rate of semi-circular surface crack normalized by energy release rate of penny-shaped crack in an infinite body at same φ for $\nu = 0.3$. The applied stress is σ_{12}^0. A comparison is shown between the predictions of two meshes with the same number of elements but differing refinement near the corner where the crack meets the free surface at $\varphi = 0$.

resolution of the intensity factors within about $\varphi = 0.05(\cong 2.5^\circ)$ of the corner. The fine mesh with the more uniformly distributed spacing around the crack front was used in the following.

2.4. Stress intensity distributions

The main results for semi-elliptical surface cracks are given in Fig. 6 and Fig. 8. Stress intensity factor distributions for $c/a = 1$, 1.5 and 2 are plotted in Fig. 6(a) for $\nu = 0.2$ and in Fig. 6(b) for $\nu = 0.3$. The intensity factors, K_{II} and K_{III}, have been normalized by the corresponding maximum values for the full elliptical crack with the same c/a and ν defined in Eq. (2) and provided in Table 1. The corresponding normalized distributions for elliptical cracks in the infinite body are plotted for comparison purposes in Fig. 7. Inspection of the reference solution (1) for the full elliptical crack, normalized by the respective maxima in Eq. (2), reveals that the normalized distributions are independent of ν (i.e. all the dependence on ν is contained in the normalizing factors, $(K^0_{\mathrm{II}})_{\varphi=0}$ and $(K^0_{\mathrm{III}})_{\varphi=\pi/2}$). The dependence on ν of the normalized distributions for the surface crack is displayed in the three plots of Fig. 8 for $c/a = 1$, 1.5 and 2. Now the role of Poisson's ratio shows up as a fairly strong influence on the stress intensity distribution near the corner at $\varphi = 0$, which is related to the effect of ν on the corner singularity discussed in Section 2.2. The influence on K_{III} is by far the largest, but this occurs in a range of φ in which K_{III} is relatively small.

Away from the corner, the role of ν on the normalized distributions is relatively small. The main

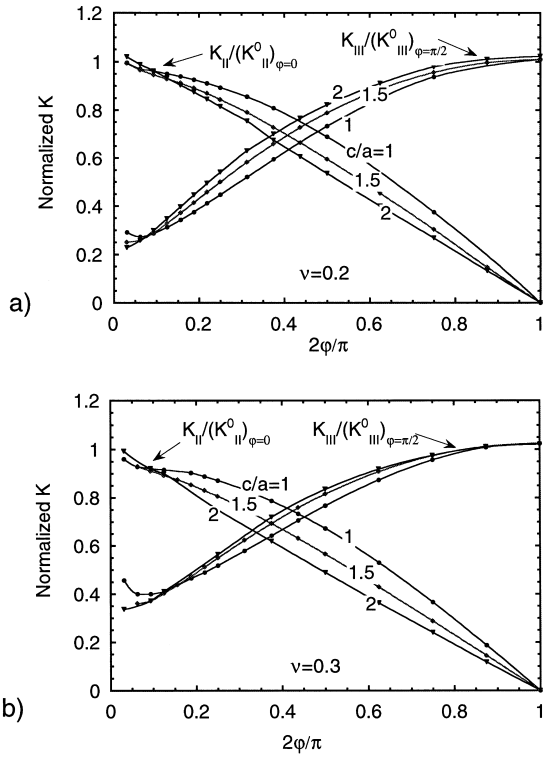

Fig. 6. Normalized distributions of the stress intensity factors for the semi-elliptical surface crack subject to nonzero σ^0_{12}: (a) $\nu = 0.2$ and (b) $\nu = 0.3$.

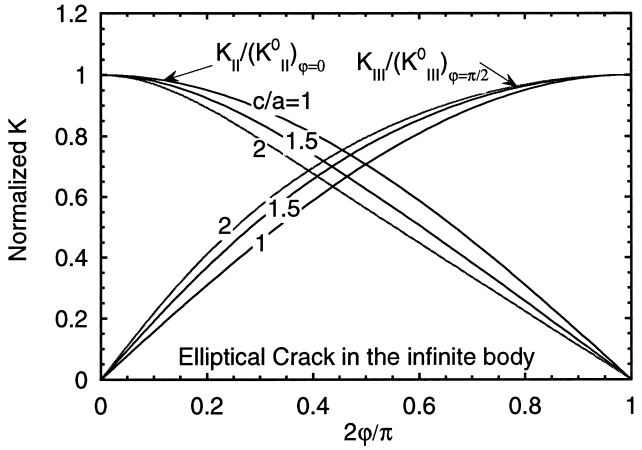

Fig. 7. Normalized distributions of the stress intensity factors for the elliptical crack in the infinite body subject to nonzero σ^0_{12}. The normalized distributions are independent of Poisson's ratio.

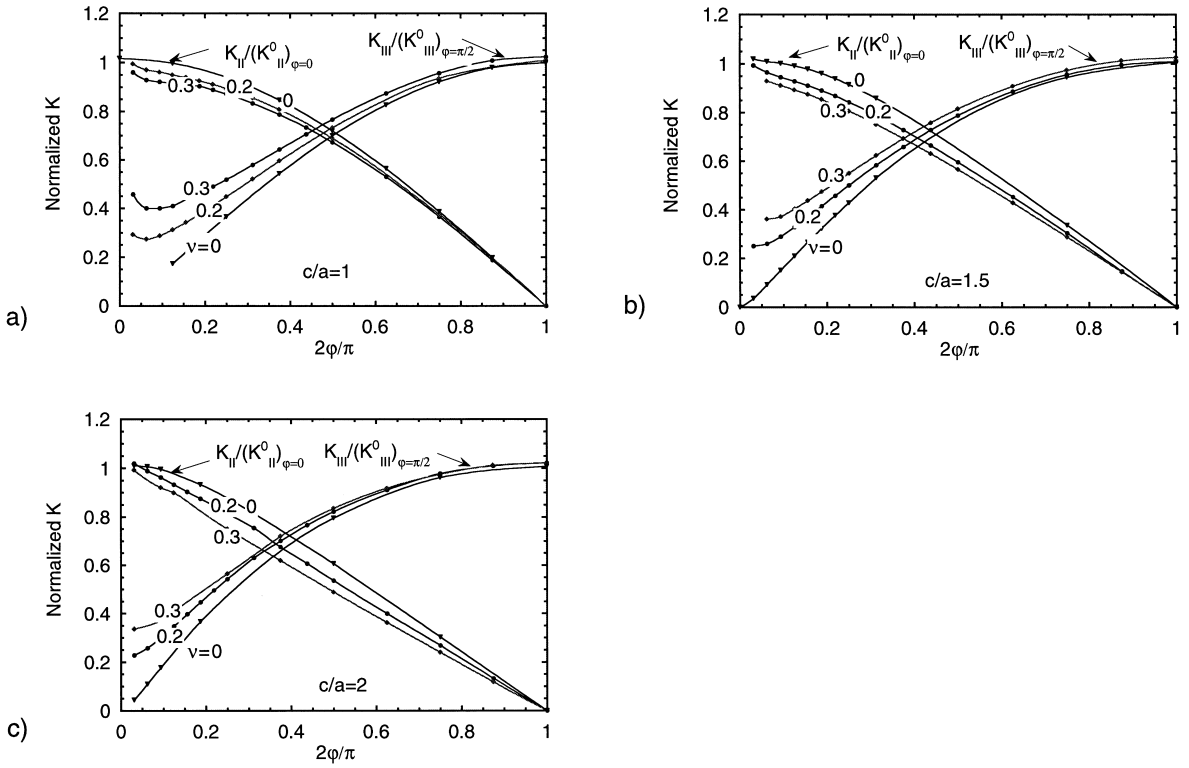

Fig. 8. Normalized distributions of the stress intensity factors for the semi-elliptical surface crack subject to nonzero σ^0_{12} for $\nu = 0$, 0.2 and 0.3: (a) $c/a = 1$, (b) $c/a = 1.5$ and (c) $c/a = 2$.

dependence of the intensity factors on ν is contained in the normalizing factors (2). Indeed, comparison of the distributions in Figs. 6 and 8 with those in Fig. 7 for the full elliptical crack in the infinite body indicates that, away from the corner, the full elliptical crack solution (1) provides a reasonably accurate approximation to problem for the semi-elliptical surface crack. The error in this approximation can be displayed by expressing the intensity factors of the surface crack as the sum of the reference intensity factors (1) and the corrections:

$$K_{\mathrm{II}} = K^0_{\mathrm{II}} + \delta K_{\mathrm{II}} \quad \text{and} \quad K_{\mathrm{III}} = K^0_{\mathrm{III}} + \delta K_{\mathrm{III}} \tag{6}$$

Values of $\delta K_{\mathrm{II}}/(K^0_{\mathrm{II}})_{\varphi=0}$ and $\delta K_{\mathrm{III}}/(K^0_{\mathrm{III}})_{\varphi=\pi/2}$ are presented as solid points in Fig. 9 for $c/a = 1.5$. The error in using Eq. (1) for the surface crack is less than 10% for the distributions in almost the entire range of φ, except for K_{III} near the corner. The error in the vicinity of the maxima of the respective

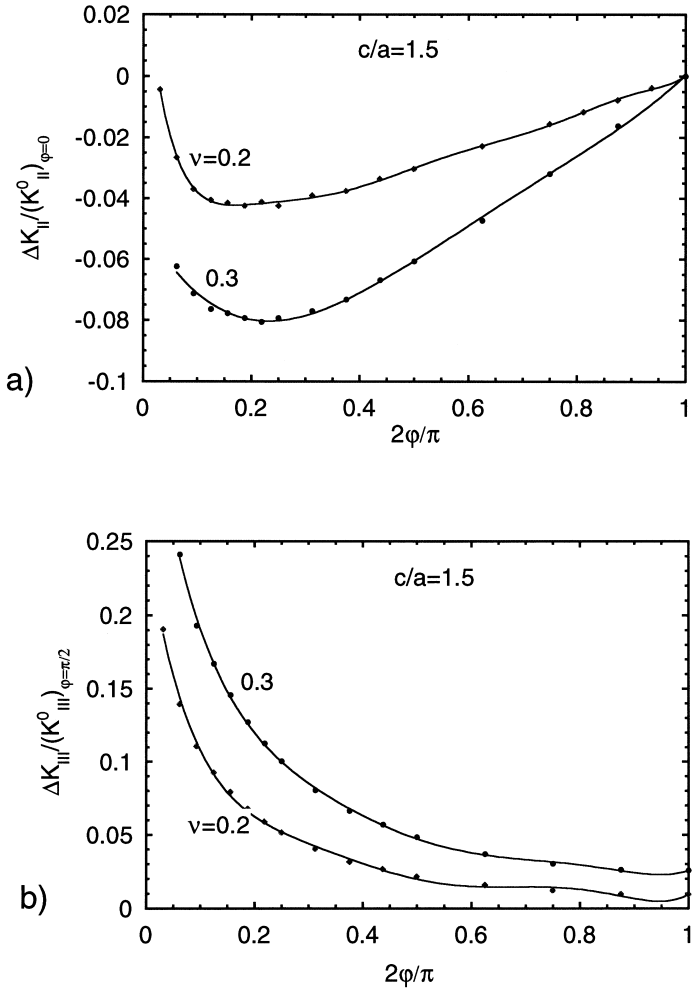

Fig. 9. Normalized distributions of the corrections to Eq. (1), defined in Eq. (6), for the semi-elliptical crack in the infinite body for the case $c/a = 1.5$. The solid points are the computed values, and the curves are the polynomial fits given in Table 2.

intensity factors is well below 5%. The trends for $\delta K_{II}/(K^0_{II})_{\varphi=0}$ and $\delta K_{III}/(K^0_{III})_{\varphi=\pi/2}$ for the other two values of c/a are similar and will not be shown. Accurate polynomial fits to the normalized corrections over the range $0.1 < \varphi \leq \pi/2$ are presented in Table 2, and these are shown for the case $c/a = 1.5$ as the curves in Fig. 9. The numerical results for the cases in this study can be reproduced using Eq. (6) with the polynomial representations in Table 2.

Murikami's [8] estimates of the stress intensity factors for the mixed mode surface crack employs what is essentially an approximation of the full elliptical crack solution. The error in this estimate can be somewhat larger than that in using the full elliptical crack solution itself.

3. Trends under mixed mode

The results presented in the previous section presenting the response of the surface crack to the applied stress component σ^0_{12} can be combined by superposition with the results of Newman and Raju [5] for the mode I contribution due to σ^0_{22}, giving the distribution of each of the three stress intensity factors along the crack front. (Recall that σ^0_{11} has no effect on the intensity factors.) Thus, for example, the energy release rate distribution associated with crack advance in the extended crack plane can be computed using the well known relation

$$G = (1-\nu^2)\left(K_I^2 + K_{II}^2\right)/E + (1+\nu)K_{III}^2/E \tag{7}$$

The general solution for the combined modes also permits one to compute energy release rates for local crack advance in directions other than in the original crack plane. In principle, the mixed mode solution contains the information required to implement any criterion for a brittle material based on local conditions in the immediate vicinity of the crack front. Several such mixed mode criteria have been widely studied and employed for cracking under monotonic loading. None are well established when the mode III component is significant.

The situation with respect to fatigue cracking is less certain under mixed mode. There seems to be general agreement, a few exceptional cases aside, that the local crack front advances under mode I conditions once it has begun to propagate. However, criteria governing threshold conditions for

Table 2
Polynominal approximations for the stress intersity factor corrections in Eq. (6)[a]

K	ν	c/a	c_0	c_1	c_2	c_3	c_4	c_5	c_6	c_7	c_8
y_{II}	0.2	1	0.0134	−0.7898	4.893	−13.94	20.63	−15.25	4.436		
y_{III}	0.2	1	0.3141	−2.851	14.08	−38.12	55.28	−40.23	11.53		
y_{II}	0.2	1.5	0.03585	−1.706	15.22	−72.67	203.8	−342.6	338.9	−181.7	40.66
y_{III}	0.2	1.5	0.2476	−2.258	11.35	−31.53	47.34	−35.81	10.67		
y_{II}	0.2	2	0.0542	−1.214	6.921	−19.95	30.58	−23.44	7.041		
y_{III}	0.2	2	0.1949	−1.452	5.474	−10.36	9.411	−3.250			
y_{II}	0.3	1	0.0153	−2.494	27.32	−143.5	421.1	−723.8	723.8	−389.7	87.34
y_{III}	0.3	1	0.5177	−4.421	22.59	−63.87	96.07	−71.99	21.13		
y_{II}	0.3	1.5	−0.0475	−0.3309	1.041	−1.063	0.4011				
y_{III}	0.3	1.5	0.3608	−2.528	10.62	−26.41	36.99	−26.72	7.715		
y_{II}	0.3	2	0.02388	−1.019	3.102	−3.975	2.401	−0.5322			
y_{III}	0.3	2	0.3341	−2.406	8.369	−14.63	12.35	−3.991			

[a] where $y = c_0 + c_1x + c_2x^2 + c_3x^3 + c_4x^4 + c_5x^5 + c_6x^6 + c_7x^7 + c_8x^8$, $x = 2\varphi/\pi$, and $y \equiv y_{II} = \delta K_{II}/(K^0_{II})_{\varphi=0}$ or $y \equiv y_{III} = \delta K_{III}/(K^0_{III})_{\varphi=\pi/2}$.

initiating fatigue crack growth under mixed mode cyclic loading are not established. It seems reasonable to expect that the threshold stress intensity factor, $(\Delta K_I)_{TH}$, determined in a mode I test might be greater than the ΔK_I component at threshold under mixed mode cyclic loading. However, there is little data on which to base such a criterion. For example, it is not known whether the decidedly more conservative criterion based on a threshold energy release rate provides a bound. That is, does a threshold value of the cyclic variation of the energy release rate determined in a mode I test, $(\Delta G_I)_{TH}$, provide an lower bound to ΔG at threshold under mixed mode? Some recent experiments under combined mode I and II on an alloy with a very fine and relatively isotropic micro-structure [3] have suggested that $(\Delta G_I)_{TH}$ may provide a lower bound, although that conclusion must be regarded as tentative until more data is available.

As remarked above, the present results for the shear loading, when combined with those for the tensile loading [5], can be used to generate distributions along the surface crack front relevant to any potential fracture criterion. As an illustration, consider the surface crack oriented at an angle β to the applied tensile stress σ in Fig. 1(b). The applied stress components in axes aligned with the crack are

$$\left(\sigma^0_{11}, \sigma^0_{22}, \sigma^0_{12}\right) = \sigma\left(\sin^2\beta, \cos^2\beta, \sin\beta\cos\beta\right) \tag{8}$$

An issue, for example, is whether the crack orientation perpendicular to the tensile stress ($\beta = 0$) is critical for threshold fatigue crack growth when σ is cycled, or whether a mixed mode orientation gives rise to fatigue crack growth at the lowest σ. It is not possible to answer this question in the absence of a

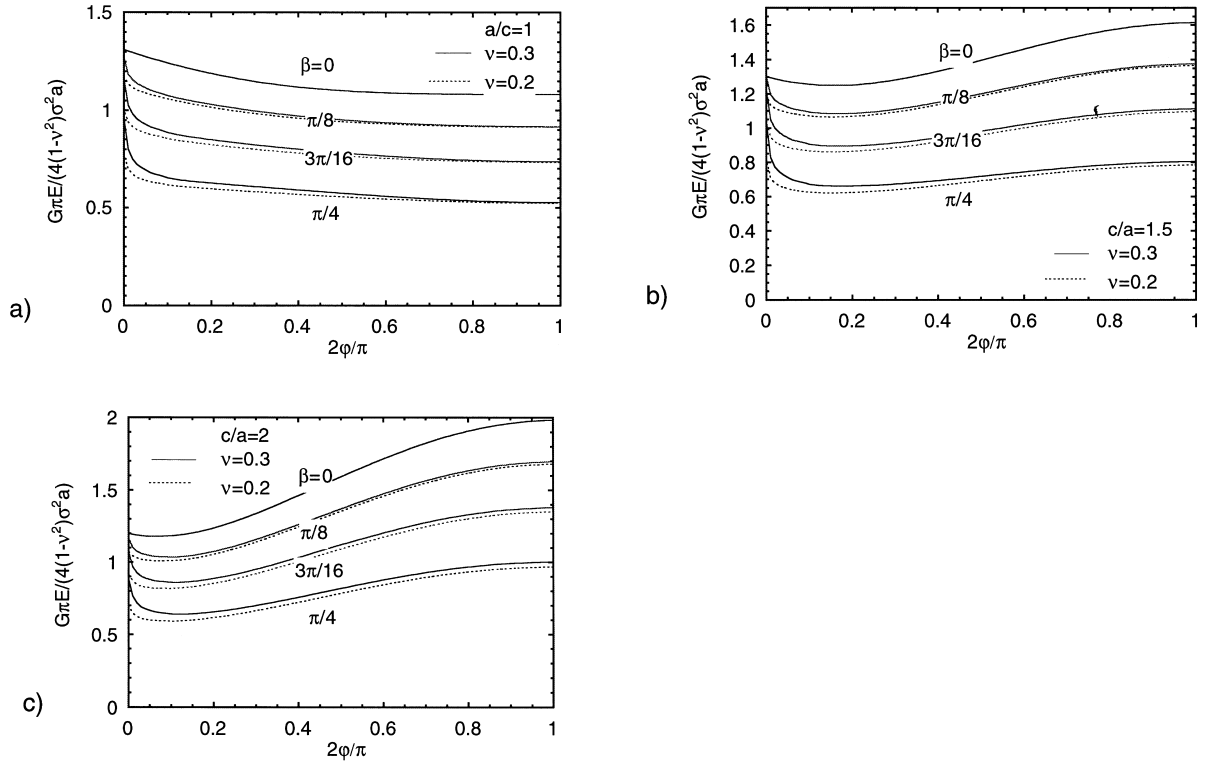

Fig. 10. Distributions of the energy release rate along the crack front for a surface crack oriented at angle β to an applied tensile stress σ: (a) $c/a = 1$, (b) $c/a = 1.5$ and (c) $c/a = 2$.

criterion for threshold under mixed mode conditions. However, examination of the energy release rate (7) distribution at various orientations can provide insight. Both K_{II} and K_{III} contribute significantly to this measure in addition to K_I, and it is plausible that $(\Delta G_I)_{TH}$ might provide a conservative threshold criterion under mixed mode. The energy release rate G has been computed using Eqs. (7) and (8) together with the distributions of K_I due to σ^0_{22} from [5] and with those for K_{II} and K_{III} due to σ^0_{12} from the data in Figs. 6 and 8 (or, equivalently, using Eq. (6) and the polynomial expressions in Table 2).

Plots of $G/[4(1-\nu^2)\sigma^2 a/(\pi E)]$ as a function of φ are shown in Fig. 10 for four orientations of the surface crack and three crack shapes. As already emphasized, values within about $\varphi = 0.05(\cong 2.5^\circ)$ from the corner at $\varphi = 0$ are not reliable. In any case, it is only the semi-circular crack for which the largest values of G occur within an appreciable vicinity of the corner. For $c/a = 1.5$ and 2, the largest values of the energy release rate occur at the point of deepest penetration of the crack at $\varphi = \pi/2$. The most notable feature for each of the three crack shapes shown in Fig. 10 is that the energy release rate distribution for the crack oriented perpendicularly to the tensile stress lies well above those for the other orientations. At a given point along the crack front, the energy release monotonically decreases as β increases. Quantitatively, similar behavior occurs for the full elliptical crack in the infinite body. If fatigue crack threshold under mixed mode were governed by $(\Delta G_I)_{TH}$, the critical orientation would be $\beta = 0$. Based on the seemingly conservative nature of the criterion based on $(\Delta G_I)_{TH}$, it would be most surprising if a surface crack at an orientation other than $\beta = 0$ were critical for threshold growth.

4. Summary

Mode II and III stress intensity factor distributions for semi-elliptical surface cracks subject to remote shear stress have been obtained for a limited range of crack ellipticity. When combined with existing results for the mode I distributions due to remote tensile stress, these results make it possible to compute critical conditions for brittle fracture initiation or fatigue crack growth threshold for any criterion requiring stresses and strains at localities near the crack front. The mode III stress intensity factor distribution, in particular, is strongly affected by a corner singularity in stresses which differs from the conventional inverse square root singularity at interior points along the front. In the vicinity of the corner, the mode III factor does not go smoothly to zero unless Poisson's ratio is zero. Apart from behavior in the vicinity of the corner, the solution (1) for the intensity factor distributions for the full elliptical crack in an infinite body provides a reasonably good approximation to the surface crack distributions for shear loading parallel to the crack. Corrections to Eq. (1) for the surface crack problem are defined in Eq. (6) and provided by polynomials given in Table 2.

Acknowledgements

This work was supported in part by the Multi-University Research Initiative on 'High Cycle Fatigue', which is funded at Harvard by AFSOR under Grant No. SA1542-22500 PG, and in part by the Division of Engineering and Applied Sciences, Harvard University.

References

[1] John B, Nicholas A, Lackey F, Porter WJ. Mixed-mode crack growth in a single crystal Ni-based superalloy. In: Lutjering G, Nowack H, editors. Fatigue '96, Proceedings of the Sixth International Fatigue Congress. Oxford: Pergamon Press, 1996. p. 399–404.

[2] John B, DeLuca D, Nicholas T, Porter J, Near-threshold crack growth behavior of a single crystal Ni-based superalloy subject to mixed mode loading. In: Miller KJ, McDowell DL, editors. Mixed mode behavior, ASTM STP 1359, ASTM, Philadelphia, PA, to be published.
[3] J. P. Campbell, A. W. Thompson and R. O. Ritchie, Mixed-mode crack growth thresholds in Ti-6Al-4V under turbine-engine high cycle fatigue loading conditions. Proceedings of the 4th National Turbine Engine High Cycle Fatigue Conference, Monterey, CA, February 1999.
[4] Raju IS, Newman Jr. JC. Stress-intensity factors for a wide range of semi-elliptical surface cracks in finite-thickness plates. Engng Fracture Mech 1979;11:817–29.
[5] Newman Jr. JC, Raju IS. An empirical stress-intensity factor equation for the surface crack. Engng Fracture Mech 1981;15:185–92.
[6] Noda N-A, Miyoshi S. Variation of stress intensity factor and crack opening displacement of semi-elliptical surface crack. Int J Fracture 1996;75:19–48.
[7] Noda N-A, Kobayashi K, Yagishita M. Variation of mixed modes stress intensity factors of an inclined surface crack. Int J Fracture, in press.
[8] Murikami Y. Analysis of stress intensity factors of mode I, II, III of inclined surface crack of arbitrary shape. Engr Fracture Mech 1985;22:101–14.
[9] Kassir MK, Sih GC. Three dimensional stress distributions around an elliptical crack under arbitrary loadings. J Appl Mech 1966;33:601–11.
[10] Sih GC, Liebowitz H. Mathematical theories of brittle fracture. In: Treatise on fracture, vol. 2. New York: Academic Press, 1998.
[11] Tada H, Paris PC, Irwin GR. The stress analysis of cracks handbook, 3rd ed., to be published by ASME.
[12] Benthem JP. State of stress at the vertex of a quarter-infinite crack in a half-space. Int J Solids Structures 1977;13:479.
[13] Bazant ZP, Estenssoro LF. Surface singularity and crack propagation. Int J Solids Structures 1979;16:661.
[14] Ghahremani F. Numerical variational method for extracting 3D singularities. Int J Solids Structures 1991;27:1371–86.
[15] Nakamura T, Parks DM. Three-dimensional elastic stress field near the crack front of a thin elastic plate. J Appl Mech 1988;55:805.
[16] Shih CF, Moran B, Nakamura T. Energy release rate along a three-dimensional crack front in a thermally stressed body. Int J of Fracture 1986;30:79–102.